Ricean K-Factor Measurements and Analysis for Wideband High-Speed Railway Channels at 2.35 GHz

Tao ZHOU[1], *Cheng TAO*[1], *Liu LIU*[1,2], *Zhenhui TAN*[1]

[1]Institute of Broadband Wireless Mobile Communications, Beijing Jiaotong University, Beijing 100044, P. R. China
[2]National Mobile Communications Research Laboratory, Southeast University, Nanjing 210096, P. R.China

11111037@bjtu.edu.cn, chtao@bjtu.edu.cn, liuliu@bjtu.edu.cn, zhhtan@bjtu.edu.cn

Abstract. *This paper presents the analysis of Ricean K-factor for wideband high-speed railway channels at 2.35 GHz, based on radio channel measurements under viaduct and U-shape cutting scenarios. We characterize the K-factor from the perspective of narrowband, wideband and delay, according to the measured channel responses. The time-frequency varying narrowband K-factors in two scenarios are analyzed and compared. A distance-based statistical narrowband K-factor model that covers the frequency variability is proposed. Then, the channel bandwidth dependent property of the wideband K-factor is investigated and we establish a simple bandwidth-based wideband K-factor model. Moreover, the K-factor for each delay bin is discussed. These results are provided for use in wireless system design and channel modeling of high-speed railway.*

Keywords

High-speed railway, Ricean K-factor, channel measurement, viaduct, U-shape cutting.

1. Introduction

In recent years, train-ground wireless communications have become a much-discussed topic with the rapid and tremendous development of high-speed railway (HSR). In order to accommodate the growing demands for communication data services, International Union of Railways (UIC) has confirmed that the existing railway control system, Global System for Mobile Communication Railway (GSM-R), will be evolved smoothly into the wideband communication system, Long-Term Evolution for Railway (LTE-R). The accurate knowledge of radio wave propagation and channel fading property is the basis of the communication network design. On the one hand, network deployment needs the radio wave propagation model to perform coverage prediction and interference analysis, on the other hand, system evaluation requires the channel fading model to accomplish performance simulation and algorithm verification. As we know, channel sounding is the most straightforward method to obtain the propagation and fading characteristics. Therefore, the channel measurement in realistic scenarios is the significant prerequisite for researches on HSR communications [1].

The wireless fading signal in HSR environments is commonly assumed to follow the Ricean distribution, due to the frequent presence of the line-of-sight (LOS) situation. Ricean K-factor is a popular parameter to quantify the channel fading severity, which is defined as the power ratio of LOS components to multipath components. An accurate characterization of the K-factor is useful for the system design such as link budget calculation, adaptive receiver design and optimal loading for transmit diversity. Besides, it is also particularly important for the radio channel modeling. Hence, the K-factor for HSR channels needs to be deeply analyzed.

However, researches on the K-factor under HSR circumstances are lacking. The WINNER II D2a model [2] provides a K-factor model for HSR channel simulations, whereas it is not based on measurement results derived from the realistic HSR environment. Extensive channel measurements using the GSM-R excitation signal at 930 MHz have been taken along the Zhengzhou-Xi'an (ZX) HSR in China [3] [4]. The narrowband K-factor in the viaduct and U-shape cutting scenario has been analyzed. It shows strong dependence on the viaduct height and the cutting width. The wideband K-factor results for HSR plain scenarios at 2.1 GHz are briefly reported in [5], which is based on channel measurements performed by the Wideband Code Division Multiple Access (WCDMA) dedicated cellular network. Authors in [1] first conducted the wideband measurement using a standard channel sounder on Beijing-Tianjin (BT) HSR in China under a viaduct at 2.35 GHz and established a position-based wideband K-factor model. The measured viaduct belongs to a relatively ideal HSR scenario with the open and clear propagation condition. However, there is another common viaduct scenario that has some scatterers such as trees and buildings needing to be concerned more [6]. In addition, the property of the K-factor in the indoor part of high-speed train has been statistically analyzed in [7].

Owing to the limitation of measurement methods or the deficiency of experimental data, the K-factor characteristics for HSR scenarios still have not got a comprehensive under-

standing, e.g., the variation of the K-factor over frequency and the bandwidth dependent property of the K-factor. On the other hand, the K-factor models proposed in previous literatures are just related to either the narrowband or the wideband K-factor. As we know, the former is employed by geometry based statistical model (GBSM) applied to system level simulations, while the latter is used in tap delay line (TDL) or cluster delay line (CDL) based model developed for system conformance tests. Thus, both types of the K-factor need to be considered. The primary contribution of this paper is to characterize the K-factor for HSR channels based on the measurement data collected in two typical scenarios on ZX line, viaduct and U-shape cutting. Variations of the narrowband K-factor over time and frequency are analyzed and compared in the scenarios. We develop a distance-based statistical model covering the frequency variability. Then, the wideband K-factor with regard to various channel bandwidths is investigated and a simple bandwidth-based model is proposed. In addition, the K-factor for each delay bin is discussed. These results will provide required information for the system design and channel modeling of the future LTE-R.

The remainder of this paper is organized as follows. In Section 2, we describe the measurement campaigns. Then, the method of extracting the K-factors is provided in Section 3. After that, Section 4 presents the data analysis and results. Finally, the conclusion is drawn in Section 5.

2. Measurement Description

2.1 Measurement System

Elektrobit Propsound [8], a standard wideband radio channel sounder, is employed in ZX HSR measurements. The measurement link from base station (BS) to relay station (RS) whose antenna (HUBER+SUHNER [9]) is placed on the top of the train has been set up. At the transmitter (Tx), a pseudo-noise (PN) sequence is periodically transmitted by a vertical-polarized dipole antenna. The chosen measurement frequency band is between 2.3 and 2.4 GHz, which has been allocated to the LTE dedicated network for railway coverage. At the receiver (Rx), the channel impulse response (CIR) is recovered by correlating the received excitation signal with a sequence copy identical to the one used at the Tx. The synchronization between the Tx and Rx employs the external GPS clock source instead of the local rubidium clock, which ensures the measurement efficiency and accuracy. Meanwhile, the real-time information of the train position and velocity is recorded by the GPS equipment. The specific measurement configuration is shown in Tab. 1.

2.2 Measurement Scenario

Viaduct and U-shape cutting are the two typical HSR scenarios which make up the most parts of ZX line. The measured scenarios and corresponding surroundings are shown in Fig. 1 and Fig. 2, respectively. From Fig. 1, there are two main categories in classification of local scatterers being around the viaduct as follows: short sparse trees and high dense trees. The latter is much higher than the surface of the train roof. Especially, the small antenna height difference between the Tx and Rx is employed in our experiments, which could cause the instantaneous and alternating shadowing between the Tx and Rx. Such a viaduct scenario leads to a worse propagation environment compared with the one measured in [1]. However, it is more realistic because passengers who expect to access cellular networks may often suffer from this kind of shadowing. The U-shape cutting is a unique HSR scenario that has the semi-closed structure covered with lots of vegetation, as shown in Fig. 2. It belongs to one type of deep cutting because the train rooftop antenna is lower than steep walls on both sides of the railway [6]. In this case, the Rx will receive rich reflecting and scattering waves introduced by the two slopes. In addition, a bridge spanning the cutting will block the radio waves in a short distance.

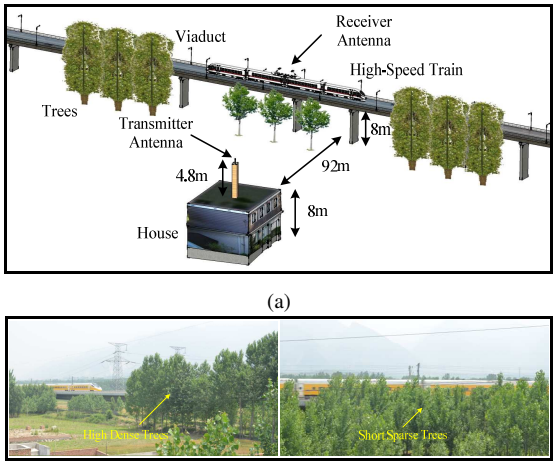

(a)

(b)

Fig. 1. The measured viaduct scenario and surrounding; (a) the propagation scenario, (b) photo of surrounding.

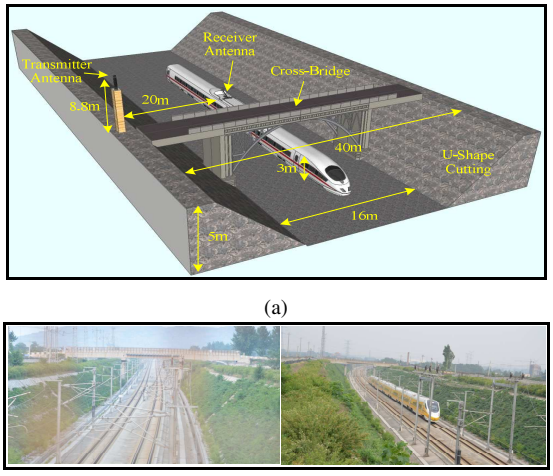

(a)

(b)

Fig. 2. The measured U-shape cutting scenario and surrounding; (a) the propagation scenario, (b) photo of surrounding.

Scenario	Viaduct	U-shape Cutting
Center frequency	2.35 GHz	2.35 GHz
Tx power	30.8 dBm	32.7 dBm
PN length	127	127
Chip rate	25 Mcps	25 Mcps
Measurement bandwidth	50 MHz	50 MHz
Channel sample rate	1968.5 Hz	1968.5 Hz
Antenna number	1×1	1×1
Tx antenna height	12.8 m	13.8 m
Rx antenna height	11 m	3 m
Averaged train velocity	200 km/h	200 km/h

Tab. 1. Measurement Parameters.

3. Extraction of Ricean K-Factor

The raw CIRs collected by Propsound cannot be directly used to extract the K-factor, due to the impact of system errors, noise components, and large-scale fading effect. In this section, we will introduce how to remove the three unfavorable factors from the measured data, and then we will show how the narrowband and wideband K-factor can be estimated.

3.1 Data Processing

Ideal wideband channel sounders should have no frequency selectivity over the entire measurement bandwidth to ensure the purity of the measured CIRs. However, it is impossible to achieve in practice because of the imperfect pulse-compression property between the transmit and receive filter [10], which can be represented as

$$P_{Tx}(f) \cdot P_{Rx}(f) \neq 1 \tag{1}$$

where $P_{Tx}(f)$ and $P_{Rx}(f)$ denote transfer functions of the transmit and receive filter, respectively. To eliminate the pulse-compression error, the raw channel data need to be compensated according to

$$H_c(t,f) = \frac{H_r(t,f)}{P_{Tx}(f) \cdot P_{Rx}(f)} \tag{2}$$

where $H_c(t,f)$ denotes the calibrated channel frequency response (CFR), which also can be transformed into CIR by IFFT.

Generally, the measured CIRs combine both effective multipath components and non-effective noise components. In order to ensure the estimation accuracy of the K-factor, we should isolate the multipath components from the data depending on a reasonable threshold. With the variation of SNR during the measurements, the noise floor of CIRs will be changed continuously. If the threshold is fixed, the decision of multipath components could be incorrect. In this paper, we rely on a dynamic noise floor identification approach [11] to deal with the CIRs. When the power of CIR tap is lower than the threshold, it will be set to zero.

Because the K-factor is a parameter that characterizes the channel small-scale fading, the effect of large-scale fading composed of path loss and shadowing should be removed before estimating the K-factor. Here, the calibrated CIR is normalized to its local root mean square (RMS) value, expressed as

$$h_{norm}(t,\tau) = h(t,\tau) / \sqrt{P_a(t)} \tag{3}$$

where $P_a(t)$ denotes the average power of CIR, which can be calculated by a sliding window with the length of N according to

$$P_a(t) = \frac{1}{N} \sum_{n=1}^{N} \int_{\tau} |h_c(t,\tau)|^2 d\tau. \tag{4}$$

N is recommended to 10 wavelengths with the distance of 1.28 m at 2.35 GHz [12].

3.2 K-Factors Estimation

Based on the processed channel data involving the CIRs and the corresponding CFRs, both narrowband and wideband K-factor can be estimated. Firstly, we need to search for the strongest path in the CIRs, and shift it to the origin. Then, the measured wideband channel could partition into multiple narrowband sub-channels according to

$$H(t,k\Delta f) = \int_{\tau} h_{norm}(t,g\Delta\tau) \exp(j2\pi f\tau)\, d\tau \tag{5}$$

where $\Delta\tau$ and g are the measurable delay resolution and the number of delay bins, respectively. k is the number of the partitioned sub-channels, $k = g-1$. Δf is the bandwidth of the sub-channel. A moment-based K-factor estimator [13] can be used when Δf is narrower than the correlation bandwidth of the actual channel. Thus, the narrowband K-factor with different frequencies is obtained based on the CFRs of each sub-channel according to

$$\hat{K}_n(t,f_k) = \frac{\sqrt{E^2(P_k) - Var(P_k)}}{E(P_k) - \sqrt{E^2(P_k) - Var(P_k)}} \tag{6}$$

where $E(\cdot)$ and $Var(\cdot)$ denote the expectation and variance of $(\cdot)$, respectively. f_k is the frequency of the kth sub-channel. P_k is the power of the CFR, which can be represented as

$$P_k = |H(t,k\Delta f)|^2. \tag{7}$$

Furthermore, different sub-channels are able to combine into the wideband channel with the optional bandwidth of $i\Delta f$, given as

$$h(t,L\Delta\tau_i) = \int_{f} H(t,i\Delta f) \exp(j2\pi f\tau)\, df \tag{8}$$

where i is the number of combined sub-channels, $i \leq k$. $\Delta\tau_i$ and L are the delay resolution of the incorporate wideband channel, $\Delta\tau_i = 1/i\Delta f$, and the corresponding number of delay bins, $L = i+1$, respectively. Similarly, we can acquire the wideband K-factor with different bandwidths and different delay bins based on the CIRs of each reconstructed wideband channel according to

$$\hat{K}_w(t,\tau_l) = \frac{\sqrt{E^2(P_L) - Var(P_L)}}{E(P_L) - \sqrt{E^2(P_L) - Var(P_L)}} \quad (9)$$

where τ_l denotes the l th delay bin, P_L is the power of the CIR, which can be expressed as

$$P_L = |h(t, L\Delta\tau_i)|^2. \quad (10)$$

The aforementioned process of channel partitioning and combining is shown in Fig. 3 when $t = t_0$. According to computer simulations, we find that the delay spread of the channel does not change in this process. But, the number of identifiable delay bins decreases due to $\Delta\tau_i > \Delta\tau$. Also, the K-factor will be different with the variation of delay resolution or channel bandwidth.

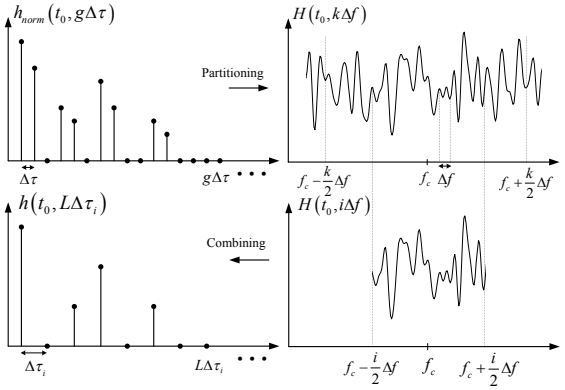

Fig. 3. The process of channel partitioning and combining.

4. Data Analysis and Results

Based on the channel data collected on ZX HSR, the 2.35 GHz Ricean K-factor characteristics in the viaduct and U-shape cutting scenarios are analyzed and compared. Major results are presented in detail as follows.

4.1 Narrowband K-Factor

Since the LTE-R standard is OFDM based, the K-factor for each sub-carrier channel needs to be studied. Also, the narrowband K-factor is one of the most important parameters in GBSM. Here, we focus on the narrowband K-factor in the range of 20 MHz bandwidth. By (5), we divide the measured channel into 253 sub-channels with 197.6 KHz each. According to [14], the maximum delay spread for typical urban models is 991 ns, corresponding to the minimum correlation bandwidth of 200 kHz. It is obvious that the LOS-dominant HSR channels have a higher correlation bandwidth. Thus, it meets the requirement of (6). Then, we extract the narrowband K-factor with the duration of 30 s for 101 sub-channels from 2.34 to 2.36 GHz, as shown in Fig. 4. High mobility in HSR scenarios is the reason that results in the time-variant of the K-factor. Since the propagation environment between the transmitter and the receiver changes rapidly, the K-factor undergoes a great variation in a short time. On the other hand, the wideband channel will appear frequency selectivity due to the effect of a multipath. The fading on each sub-channel is different, thus leading to the K-factor variation over frequency. In fact, it is hard to predict which frequency has the higher K-factor. Instead, the K-factor at a certain time or location can be understood intuitively according to the actual propagation conditions. The effective approach to determine the "good" frequency is based on field channel measurements. From Fig. 4(a), it is noted that the K-factor at 2.34 – 2.346 GHz is higher than that at other frequencies. This means 2.34 – 2.346 GHz is the preferred frequency in our measured scenario. If we consider the operating frequency for deployment of communication systems, the 2.34 – 2.346 GHz may be the better choice than other frequencies.

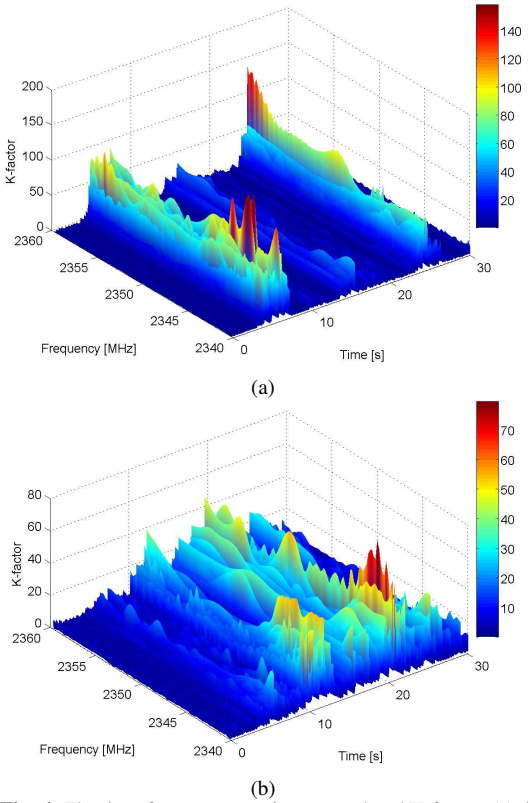

Fig. 4. The time-frequency varying narrowband K-factor; (a) the viaduct scenario, (b) the U-shape cutting scenario.

In order to further analyze the time variability of the narrowband K-factor, we first isolate the time-dependent component of the K-factor, called K_t, which is computed by averaging the K-factors on all sub-channels. Then, K_t is transformed into the K-factor as a function of distance, expressed as K_d. Fig. 5 shows the narrowband K-factor against the relative horizontal distance between the Tx and Rx (T-R distance) in the two scenarios. From Fig. 5(a), we find that the fading property in the viaduct scenario is apparently changing as the train passes through the Tx from –800 to 800 m. When the T-R distance is about ±500 m, the strength of the K-factor could reach as high as 20 dB. Then, the K-factor value drops gradually and fluctuates between -5 and 5 dB when the train arrives at the ±250 m region. The propagation condition in this area can be regarded as non-line-of-sight (NLOS) as the direct ray is completely obstructed by

the high dense trees. Especially, when the train runs close to the Tx, the K-factor has the medium strength that intensively changes from 5 to 10 dB, rather than reaching at the peak like the phenomenon in [1]. This is because the short sparse trees partially block the fixed path, resulting in an obstructed-line-of-sight (OLOS) propagation situation. Thus, the alternating propagation environment including LOS, OLOS and NLOS causes the fast fading variation in the case of the high mobility, which could affect the performance of wireless communication receivers.

Compared with the viaduct scenario, the U-shape cutting scenario has a more stable fading variation, as shown in Fig. 5(b). It is observed that the K-factor decreases over the T-R distance. This is notably due to the strength of multipath components varying far less than the strength of specular components [15]. Moreover, the K-factor experiences a precipitous decline and then rises again. This is because the cross-bridge blocks the propagation path and causes a temporal NLOS situation. We also find that although the U-shape cutting is a LOS-dominant scenario, the K-factor in such a scenario is lower than that in the viaduct LOS region. The reason is that the special U-shape structure produces a lot of reflecting and scattering waves that reduce the effect of fixed components, whereas the viaduct unobstructed region has the pure LOS propagation condition. Especially, there is the similar K-factor result for the whole U-shape cutting terrain and the viaduct OLOS region. Therefore, we infer that the fading of the deep cutting scenario could be equivalent to that of the partially obstructed viaduct scenario.

To characterize the narrowband K-factor over T-R distance, we perform the Gaussian function fitting using the Least Squares (LS) method, as shown in Fig. 5 by blue lines. For the viaduct scenario, three Gaussian functions are applied to the LOS and OLOS segments, and two juncture areas of the functions are represented for the NLOS segments. For the U-shape cutting scenario, only one Gaussian function is employed. The temporal NLOS case is not considered. Hence, a distance-based statistical model is proposed as

$$K'_{n,dB}(d) = K_{n,med}(d) + x\sigma_d \tag{11}$$

where $K_{n,med}(d)$ denotes the mean value of K_d, expressed by the fitting function as follows:

$$K_{n,med}(d) = \sum_{m=1}^{M} a_m \exp\left[-\left(\frac{d-b_m}{c_m}\right)^2\right], \tag{12}$$

M is the amount of LOS and OLOS regions and m is the index, a_m denotes the peak value of the Gaussian function, b_m represents the relative horizontal distance between the specific propagation region and TX, c_m is associated with the region width, x is zero-mean Gaussian variable with the unit standard deviation. σ_d denotes the standard deviation. In order to acquire σ_d, we normalize the estimated K_d with the median values given by (12), and then compute the cumulative distribution function (CDF) of the median-normalized K-factors on a probability scale as shown in Fig. 6(a) and (b). It is known that the closeness to a straight line on this scale implies a lognormal distribution. Thus, we obtain that the corresponding standard deviations are 4.04 and 3.59 dB in the viaduct and U-shape cutting scenarios, respectively.

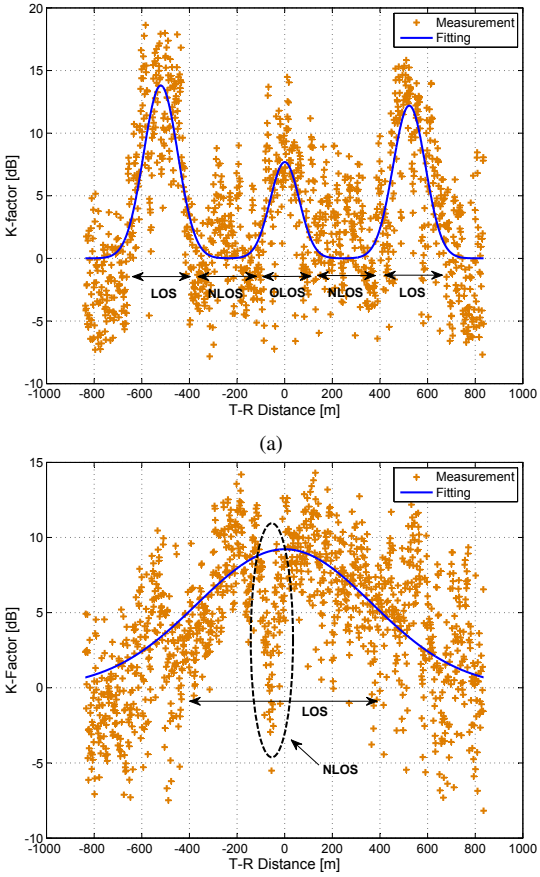

Fig. 5. The narrowband K-factor against T-R distance; (a) the viaduct scenario, (b) the U-shape cutting scenario. The positive distance means the train moves away from the Tx, while negative distance means the train runs towards the Tx. The divided LOS, OLOS, and NLOS segments are also indicated.

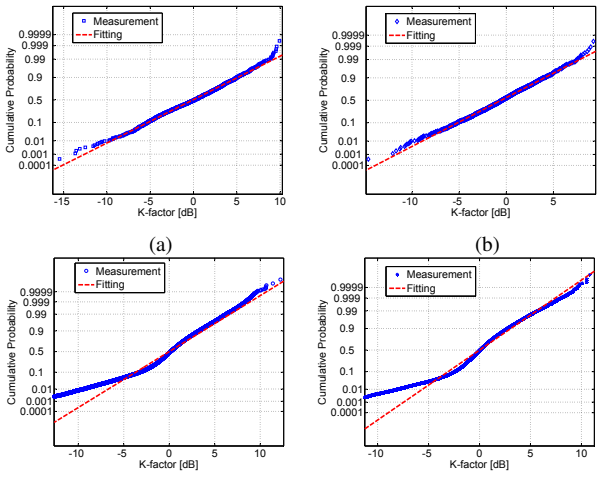

Fig. 6. CDFs of the narrowband K-factor about mean values; (a) K_d about mean in viaduct, (b) K_d about mean in cutting, (c) K_f about mean in viaduct, (d) K_f about mean in cutting.

Type	Narrowband K-factor model						Wideband K-factor model			
Parameter	m	a_m [dB]	b_m [m]	c_m [m]	σ_d [dB]	σ_f [dB]	p_3	p_2	p_1	σ_b [dB]
Viaduct	1	13.8	-520.2	101.4	4.04	2.87	-0.0107	0.5233	4.62	5.608
	2	7.685	0.5103	86.42						
	3	12.19	523.3	96.15						
U-shape cutting	1	9.22	0.3612	519.5	3.59	2.41	-0.0082	0.4708	5.37	5.238

Tab. 2. Narrowband and wideband K-factor model coefficients for viaduct and U-shape cutting scenarios.

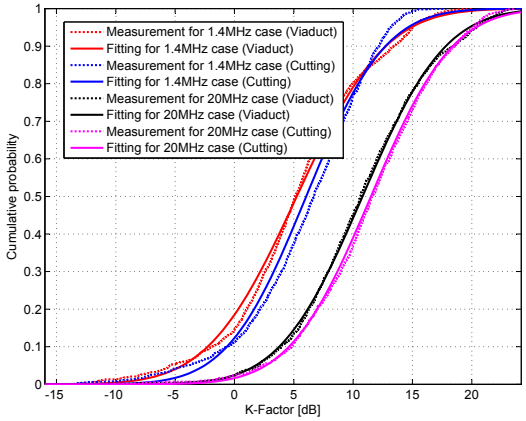

Fig. 7. The CDFs of the wideband K-factor with 1.4 and 20 MHz bandwidth in viaduct and U-shape cutting scenarios.

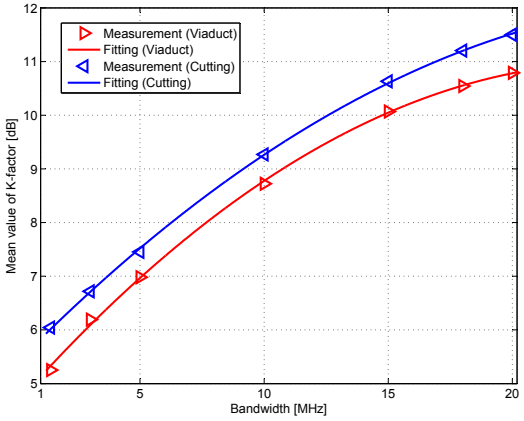

Fig. 8. The median of the wideband K-factor against channel bandwidth in viaduct and U-shape cutting scenarios.

In addition to the time variability of the narrowband K-factor, the frequency variability also needs to be considered. The frequency-dependent component of the K-factor is defined as K_f. We subtract the corresponding K_t from the K-factors on all sub-channels, and then combine all the data together in a common group. Fig. 6(c) and (d) show the CDFs of K_f about the mean values. It can be found that the cumulative probability between 1 % and 99 % is approximately close to a straight line. This confirms the lognormal property of the frequency-dependent K-factor. The slopes of the straight lines indicate the corresponding standard deviation (expressed as σ_f) of 2.87 dB and 2.41 dB for the viaduct and cutting scenarios, respectively. According to the similar standard deviations, we conclude that the narrowband K-factor in the obstructed viaduct and deep cutting scenario has the parallel frequency variability.

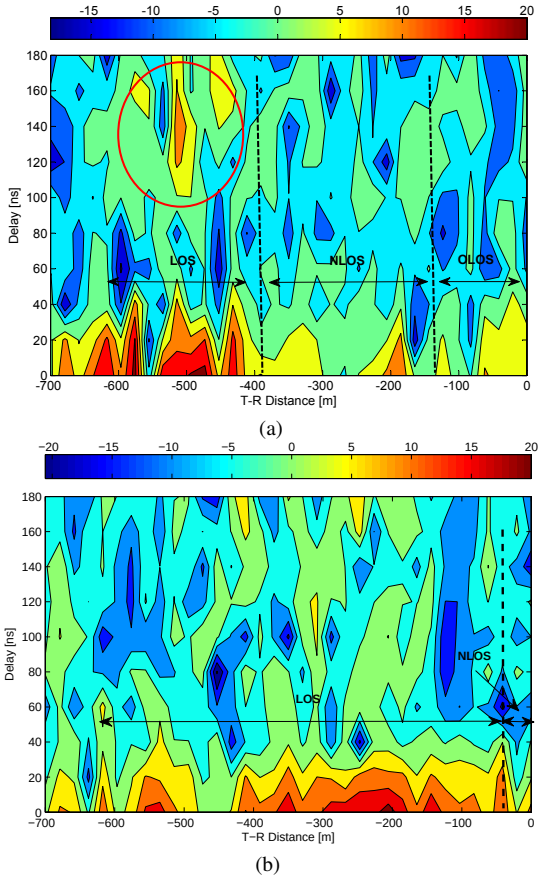

Fig. 9. The delay K-factor against T-R distance. (a) The viaduct scenario. (b) The U-shape cutting scenario.

Finally, the narrowband K-factor model considering both the time and frequency variability for the measured HSR channels at 2.34 – 2.36 GHz is written as

$$K_{n,dB}(d) = K_{n,med}(d) + x\sigma_d + y\sigma_f \tag{13}$$

where y is the zero-mean Gaussian variable with the unit standard deviation and is independent with x. Tab. 2 lists the narrowband K-factor model coefficients.

4.2 Wideband K-Factor

The wideband K-factor is regarded as a parameter of the strongest path for the LOS condition in TDL/CDL based channel models. In this section, we no longer discuss its time-frequency variability the same as the narrowband K-factor. Instead, our aim is to learn the channel bandwidth dependent property of the wideband K-factor.

According to the combination of 7 and 100 sub-channels, the CIRs with 1.4 and 20 MHz bandwidths can be

acquired by (6), respectively. Then, we estimate the wideband K-factor for the first delay bin by (7), and compute the CDFs as shown in Fig. 7. It is seen from the fitting results that the distributions of the K-factor with both bandwidths in the two scenarios are very nearly Gaussian. The median of the 20 MHz K-factor is higher than that of the 1.4 MHz K-factor. There are more NLOS sub-paths separating from the fixed path due to the higher channel bandwidth. In this case, the reduction of power of scattering components in the first delay bin causes the stronger wideband K-factor.

In order to investigate the bandwidth-dependent property, we consider the wideband K-factor with multiple bandwidths. Here, the chosen bandwidths are the same as LTE system bandwidths, i.e., [1.4, 3, 5, 10, 15, 18, 20] MHz. In Fig. 8, the median of the wideband K-factor as a function of channel bandwidth is plotted. It is obvious that the median increases with the channel bandwidth. And there are similar changing tendencies for the two scenarios. The median in the cutting environment is a little higher than that in the viaduct environment. Moreover, we find that it has a linear rise in the range of 1.4 – 10 MHz, while the rising tendency is gradually slowing between 10 and 20 MHz. Therefore, we employ a polynomial function to fit the median. Then we establish a wideband K-factor statistical model composed of a bandwidth-based median and a standard deviation that describes the K-factor variation, expressed as

$$K_{w,dB}(b) = K_{w,med}(b) + z\sigma_b \tag{14}$$

where

$$K_{w,med}(b) = p_3 b^2 + p_2 b + p_1, \tag{15}$$

b is the bandwidth in MHz, y is the zero-mean Gaussian variable with the unit standard deviation. The wideband K-factor model coefficients are also listed in Tab. 2.

4.3 Delay K-Factor

As we know, the TDL/CDL model for terrestrial cellular channels commonly considers the K-factor of the strongest path, and ignores that of the other paths. However, it is reported in [1] that in HSR viaduct propagation environments, the K-factor is not simply confined in the first LOS path, but exists in the second and third resolvable NLOS paths. Hence, we expect to recognize whether this phenomenon appears in our measured viaduct and U-shape cutting scenarios.

Fig. 9 illustrates the delay-varying K-factor at 20 ns intervals over the T-R distance. Note that the extracted K-factor is based on the channel data without removing the noise components. Here, we neglect the K-factor below 0 dB because it is not obtained by the effective multipath components. It can be seen that the strongest K-factor always occurs at the beginning of the delay bins in both scenarios. This is because the LOS ray is always the first one that arrives at the receiver in the measured scenarios, and it has the most obvious fixed component among arriving waves, which can give rise to the large K-factor. We can also find that there exists a strong K-factor up to 5 – 10 dB around the delay of about 140 ns when the train arrives at the LOS region in the viaduct scenario, as shown in Fig. 9(a). This confirms that in addition to the LOS path, the dominating component could exist in the NLOS paths. This result is consistent with that in reference [1] where the K-factor of the first resolvable NLOS path is modeled by a normal distribution. The mean value is 5.9 dB with a standard deviation of 1.7 dB.

However, there is no apparent K-factor existing in other delay bins for the obstructed viaduct regions and the whole U-shape cutting terrain. This is due to the stronger power of the reflecting and scattering components in these environments. In this case, the power of the specular component in the NLOS path seems not strong enough compared with that of the other reflecting and scattering components, which will cause a very low K-factor that can be ignored. Thus, we can conclude that the K-factor in other delay bins needs to be concerned only if the train is under the strong LOS but rare reflection and scatter situation, such as the open and clear viaduct environment.

5. Conclusion

In this paper, we have presented the measurements and analysis of the short-term fading behavior in the typical HSR scenarios, focusing on the Ricean K-factor of the wideband radio channel. The results of the K-factor from narrowband, wideband and delay aspects have been reported. The narrowband K-factors with the strong variations over the time and frequency in the two scenarios are characterized and compared. It shows that the fading of the deep U-shape cutting scenario could be similar to that of the viaduct scenario with partial shadowing. And we establish a distance-based statistical model that takes the frequency variability into account to predict the narrowband K-factor on different carrier frequencies and train positions. Then, we analyze the wideband K-factor with various channel bandwidths, whose median shows the increasing tendency over the bandwidth. Also, a simple bandwidth-based wideband K-factor model is proposed. Furthermore, according to the delay K-factor result, we conclude that the obstructed viaduct and deep U-shape cutting scenarios, unlike the open and clear viaduct environment, have no obvious K-factor exists in the other resolvable NLOS paths. The analysis results will be applicable to the design of future HSR communication systems and the modeling of HSR channels.

Acknowledgements

The research was supported in part by the NSFC project under grant No. 61371070 and No. 61032002, the Open Research Fund of National Mobile Communications

Research Laboratory, Southeast University (No.2012D07), and the Fundamental Research Funds for the Central Universities under grant No.2012JBM005.

References

[1] LIU, L., TAO, C., QIU, J. H., CHEN, H. J., YU, L., DONG, W. H., YUAN, Y. Position-based modeling for wireless channel on high speed railway under a viaduct at 2.35 GHz. *IEEE Journal on Selected Areas in Communications*, 2012, vol. 30, no. 4, p. 834 - 845.

[2] PEKKA, K., et al. *WINNER II Channel Models; Part II Radio Channel Measurement and Analysis Results.* Technical report, 2007.

[3] HE, R. S., ZHONG, Z. D., AI, B., DING, J. Measurements and analysis of short-term fading behavior for high-speed rail viaduct scenario. In *Proceedings of the IEEE International Conference on Communications*. Ottawa (Canada), 2012, p. 4563 - 4567.

[4] HE, R. S., ZHONG, Z. D., AI, B., DING, J. Propagation measurements and analysis for high-speed railway cutting scenario. *Electronics Letters*, 2011, vol. 47, no. 21, p. 1167 - 1168.

[5] QIU, J. H., TAO, C., LIU, L., TAN, Z. H. Broadband channel measurement for the high-speed railway based on WCDMA. In *Proceedings of the IEEE 75th Vehicular Technology Conference*. Yokohama (Japan), 2012, p. 1 - 5.

[6] AI, B., HE, R. S., ZHONG, Z. D., GUAN, K., CHEN, B. H., LIU, P. Y., LI, Y. X. Radio wave propagation scene partitioning for high-speed rails. *International Journal of Antennas and Propagation*, 2012.

[7] DONG, W. H., LIU, G. Y., YU, L., DING, H. Y., ZHANG, J. H. Channel properties of indoor part for high-speed train based on wideband channel measurement. In *Proceedings of the 5th ICST Conference on Communications and Networking in China (CHINACOM)*. Beijing (China), 2010, p. 1 - 4.

[8] Elektrobit. *PropSoundTM CS Multi-Dimensional Channel Sounder General Presentation.* 2005.

[9] Huber+Suhner AG RF Industrial. *Sencity Rail Antenna: 1399.17.0039 (datasheet).* [Online] 2010. Available at: http://www.firstsourceinc.com/products/6901-23041568.aspx

[10] MATZ, G., MOLISCH, A. F., HLAWATSCH, F. On the systematic measurement errors of correlative mobile radio channel sounders. *IEEE Transactions on Communications*, 2002, vol. 50, no. 5, p. 808 - 821.

[11] ZHANG, J. H., LU, Y., XU, D., ZHANG, P., LIU, G. Y., HUANG, Y. *Method and Device of Noise Floor and Threshold Decision Estimation Based on Channel Sounding*. Chinese Patent CN 101 426 212A, 2009.

[12] DONG, L., ZHANG, J. H., ZHANG, Y., NIE, X. Large scale characteristics and capacity evaluation of outdoor relay channels at 2.35 GHz, In *Proceedings of the IEEE 70th Vehicular Technology Conference*. Anchorage (USA), 2009, p. 1 - 5.

[13] GREENSTEIN, L. J., MICHELSON D. G., ERCEG, V. Moment-method estimation of the Ricean K-factor. *IEEE Communications Letters*, 1999, vol. 3, no. 6, p. 175 - 176.

[14] 3GPP *TS 36.101 V8.4.0, User Equipment (UE) Radio Transmission and Reception*, 2008.

[15] GREENSTEIN, L. J., GHASSEMZADEH, S. S., ERCEG, V., MICHELSON, D. G. Ricean K-factors in narrowband fixed wireless channels: Theory, experiments, and statistical models. *IEEE Transactions on Vehicular Technology*, 2009, vol. 58, no. 8, p. 4000 - 4012.

About Authors ...

Tao ZHOU was born in Jiangxi Province, China, in 1988. He received the B.E. degree from Changchun University of Science and Technology, Changchun, China, in 2009. He is pursuing the Ph.D. degree of Institute of Broadband Wireless Mobile Communications, School of Electronics and Information Engineering, Beijing Jiaotong University. His general research interests include radio channel measurement, characterization and modeling for high-speed railway, design of channel sounder based on software defined radio.

Cheng TAO was born in Shanxi Province, China, in 1963. He received his M.Sc. degree from Xidian University, Xian, China, and Ph.D. Degree from Southeast University, Nanjing, China, in 1989 and 1992, respectively, all in electrical engineering. He has been with the School of Electronics and Information Engineering, Beijing Jiaotong University since 2002. He is a professor and the director of the Institute of Broadband Wireless Mobile Communications. His research interests include wireless communication systems and signal processing.

Liu LIU was born in Yunnan Province, China, in 1981. He received the B.E. and Ph.D. degrees from Beijing Jiaotong University, Beijing, China, in 2004 and 2010, respectively. From 2010, he was a post Ph.D. researcher of institute of Broadband Wireless Mobile Communications, School of Electronics and Information Engineering, Beijing Jiaotong University. He is now an associate professor of Beijing Jiaotong University. His general research interests include channel measurement and modeling under high-speed railway, signal processing of wireless communication in time-varying channel.

Zhenhui TAN was born in Jiangsu Province, China, in 1944. He received the M.S. and Ph.D. degrees in Communications and Information Systems from Beijing Jiaotong University (BJTU), Beijing and Southeast University, Nanjing, China in 1982 and 1987, respectively. From 1990 to 1993, he was a visiting scholar at Mons Technology College, Belgium and at University of Waterloo, Canada. He has been with BJTU, where from 1993 to 1995 he was a director of Department of Communications and Signal Control Engineering in BJTU. From 1995 to 1998 and from 1998 to 2008, he was a Vice President and the President of BJTU. His current research interests include digital mobile communications network, spread spectrum communications, broadband wireless access, adaptive filtering algorithms and beyond 3G system.He is the author of two books and more than 100 papers on communication and information areas. He also serves as the editor of the Chinese Journal of Electronics and the Journal of the China Railway society. Professor Tan is a Fellow of the Chinese Institute of Communication (CIC) and the Chinese Institute of Railway (CIR). He is also the Vice Chairman of the academic committee of the CIC and CIR. Professor Tan was awarded by State Excellent Coming-Back From-Abroad Scholars, Experts of Outstanding Achievements from the State Council.